10.2478/v10048-008-0018-7
MEASUREMENT SCIENCE REVIEW, Volume 8, Section 3, No. 3, 2008

Using the Diffractive Optics for 3D Inspection of Nuclear Reactor Fuel Assembly Grid Spacers

L.V. Finogenov, Yu.A. Lemeshko, P.S. Zav'yalov

Technological Design Institute of Scientific Instrument Engineering,
Siberian Branch of the Russian Academy of Sciences 41, Russkaya str., Novosibirsk, 630058, Russia
Email: chugui@tdisie.nsc.ru

Ensuring the safety and high operation reliability of nuclear reactors takes 100% inspection of geometrical parameters of fuel assemblies, which include the grid spacers fabricated as cellular structure with fuel elements. The required grid spacers' geometry of assembly in the transverse and longitudinal cross sections is extremely important for maintaining the necessary heat regime. A universal method for 3D grid spacer inspection using the diffractive optical element, which generates, as the structured light, a multiple-ring pattern on the inner surface of a grid spacer cell is investigated. The experimental measurement error for cell centers position deviation is ±7 μm, and the error for overall dimensions is ±11 μm.

Keywords: structured light method, diffractive optical element, fuel assembly, grid spacer

1. INTRODUCTION

AT THE PRESENT time, in order to provide extremely high reliability and safety of atomic power plants, rigid requirements should be imposed on the quality of nuclear reactors [1]. The equipment for atomic power plants produced in Russia by JSC TVEL is mainly designed for two types of reactors on thermal neutrons with water cooling: VVER-1000 and VVER-440 (see Fig.1).

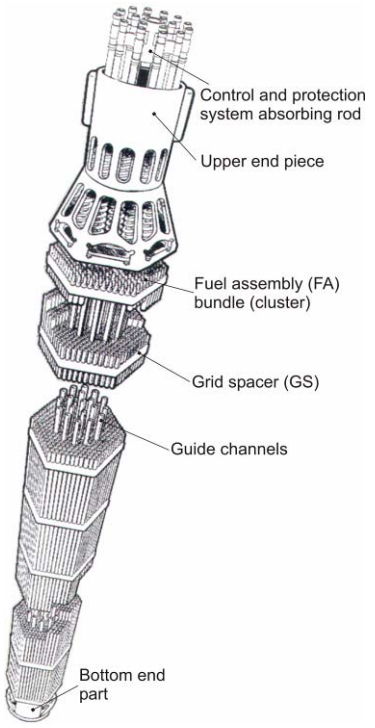

Fig.1 Fuel assembly for Russian nuclear reactor VVER-1000

The main element of these reactors is a fuel assembly (FA) of hexagonal shape, which contains several hundreds of fuel elements (with a diameter of about 9 mm and a length from 2.5 m to 4 m), grid spacers (GS), and a carrying frame. The GS (see Fig.2a) has a cellular structure with a set of fuel elements cells. The required strictly spaced arrangement of the fuel elements in cross-sections and longitudinal sections (along the FA) is specified by the grid spacers. This arrangement is extremely important for providing the thermal regime necessary for the FA operation. The configurations of cell channels and guide channels of grid spacers, the distances between their neighbouring cells, and the FA overall dimensions "for spanner" should be the subject for 100% three-dimensional (3D) inspection (the inspection time must be less than 12 min). At present, grid spacers inspection is realized by contact gauges (cylinders, balls). Such inspection does not give full information about grid spacers' geometry. The sampling inspection by coordinate-measuring machine that requires a lot of temporal expenditure (3–4 hours for one spacer grid) is used at the stage of technology working-off. The most promising available noncontact means of 3D inspection is the structured illumination method [2]. It is based on illumination of the object by a light beam with a known configuration (a line, grating, etc.), recording of the image by a CCD camera, and information processing. The shape and the geometric parameters of the object surface inside the $D_x \times D_y \times D_z$ measurement volume are reconstructed using a set of cross sections of the object. Earlier, an optoelectronic system for the inspection of grid spacers' main geometric parameters, which is based on the multipoint structural illumination, was developed [3] at TDI SIE . The system is designed for hexagonal grid spacers. A novel method for grid spacers' geometry inspection, which allows us to develop a universal, precision system for automated inspection, is considered in this work. We have proposed and developed a universal system for 3D grid spacer inspection using the diffractive optical element (DOE).

2. UNIVERSAL DOE - BASED METHOD FOR GRID SPACERS INSPECTION

The method must provide the inspection of the following grid spacers parameters (Fig.2b): diameters $\mathbf{D_c}$ of cells (~9 mm, the error $\mathbf{\delta D_c}$ must not exceed ±10 μm) formed by their three bulges-protrusions; diameters $\mathbf{D_{ch}}$ of circles inscribed

in guide channels (~13 mm, $\delta D_{ch} \leq \pm 10$ μm); distances **L** between the centers of neighbouring cells ($\delta L \leq \pm 30$ μm); displacements of the centers of inscribed circles for cells from their drawing positions (positioning displacements); FA overall dimensions "for spanner" (**B** = 140 ÷ 240 mm, $\delta B \leq \pm 100$ μm). For square grid spacers, the distances between opposite protrusions rather than diameters are inspected. The cell length is being varied within 10 – 30 mm. The protrusions length is 3 – 15mm.

a)

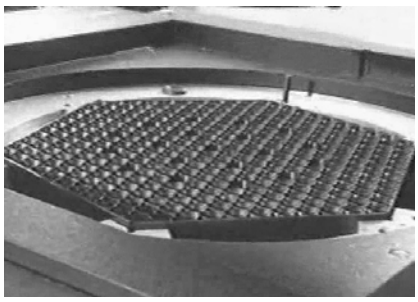

b)

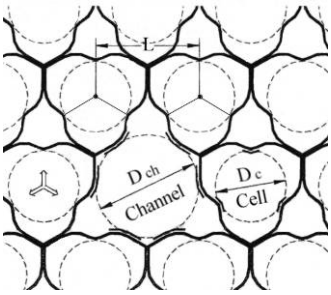

Fig.2 Configuration of grid spacer: its photo (a), object cross-section (b) with the basic inspected parameters, including cell diameter $\mathbf{D_c}$, channel diameter $\mathbf{D_{ch}}$, distance between neighbouring cells **L**

To provide the universality and metrological characteristics of the system under development, a method for inspection of grid spacers is proposed. The method is based on structural illumination of cell inner surface by multiple-ring pattern (Fig.3). A diffractive optical element is used as an illuminator part.

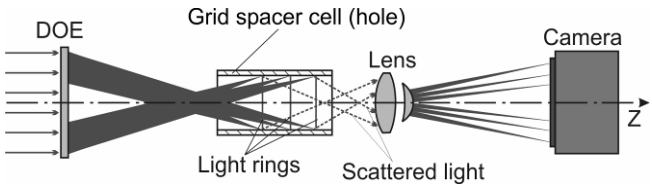

Fig.3 The grid spacer cell inspection method using diffractive optical element, which generates a set of rings located along Z-axis of the cell

In the method proposed above, the DOE focuses laser radiation to a set of rings of the same diameter located along the Z-axis of the cell with some spacing.

The illuminated surface of the cell is projected onto the photodetector matrix of the camera using a special objective with a large field curvature and distortion. The output image as a fringe pattern formed by this objective is processed by computer. In the process of measurement, the spacer is moved by a two-dimensional motorized stage in a plane perpendicular to the system optical axis. This provides measurement of all geometrical parameters of grid spacers. The method proposed above allows us to inspect all available types of grid spacers.

3. DOE SYNTHESIS

The key element of the structural illumination method proposed above is the DOE. The following requirements are specified for the DOE. To provide information reliability in the inspection along the protrusion, 10 – 15 sections should be inspected. Therefore, the DOE must form surface protrusions of 10 – 15 rings with a spacing of 0.5 – 1 mm. To inspect cells with long and short protrusions, different diffractive elements should be used. The ring focusing range in the radial direction must correspond to the assigned tolerance on the cell center location (0.15 – 0.3 mm).

Diffractive elements that focus radiation to a system of rings were developed by two ways. According to the first method, the DOE is divided into radial segments, with each segment generating one light ring. The second method is as follows: the DOE, with its entire surface, generates a set of light rings along the optical axis. In this case the DOE serves as a hologram.

For preliminary experiments, the diffractive elements of both types were developed. The segmented diffractive element generating 10 – 15 light rings must have a large diameter and focal length (of the order of D = 80 mm, F = 160 mm) for the light rings to be narrow enough. In these conditions it has a significant shortcoming: the angles of incidence for the different parts of the protrusion differ considerably. This does not provide the same conditions of measurement along the entire length of the cell. Besides, the use of a segmented DOE imposes more stringent requirements on the uniformity of the laser beam intensity. Experiments and theoretical calculations have shown that the DOE-hologram is the best solution.

a)

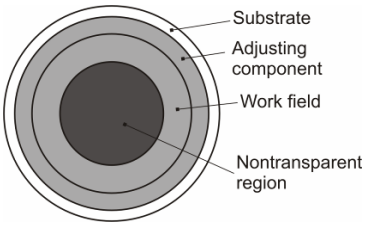

b)

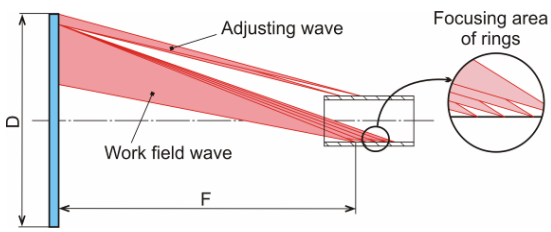

Fig.4 Diffractive optical element: structure (a), ray path for radiation (b)

The DOE-holograms were calculated on the base of Kirchhoff – Fresnel approximation [4] and produced at TDI SIE by a circular laser photoplotter CLWS-300/C-M [5] using a thermochemical technology based on diffractive structure recording on glass substrates coated by chromium film and its subsequent liquid etching. The photoplotter has the following characteristics: maximum diameter of the working field is 300 mm, the resolution of the radial coordinate is 0.6 nm, and the resolution of the angular coordinate is 0.5 angle/s. The diameter of the manufactured DOEs is equal to 45 mm, and the working wavelength is 660 nm. The minimum period of diffraction zones is equal to 1μm. Fig.4a) shows the structure of such a hologram. It has three zones: nontransparent region (24 mm diameter), work field (6.5 mm ring width) and adjusting component (4 mm ring width).

Besides a working field, the DOE has a nontransparent zone in the center and an additional adjusting component at the periphery. The nontransparent zone in the center has several functions. First, it does not transmit direct laser radiation to the projection objective. Second, this zone decreases the angular aperture of the work field and, therefore, the surface is illuminated by a radiation that does not contain grazing rays. The adjusting component of the DOE generates two rings, whose diameters are the same as from the working field (see Fig.4b), but the ray path is different. The rays do not intersect the optical axis. Thus, if the inspection zone has a grid spacer cell, these rays do not come to the projection objective aperture, so the adjusting rings are not visible. When there is no cell, the radiation from the DOE work field scattered from the cell does not get to the objective aperture, and two adjusting rings appear, using which one can align the receiving optical part with respect to the illuminating optical system. As for the calibration procedure under cell measurement, we used the precision cylinder workpieces with various diameters. The alignment of axis cell relative to the axis of optical system occurs only in case if their misalignment is greater than the zones of the DOE working field focusing in radial direction 0.15 – 0.3 mm. Figure 5 shows intensity distributions formed by the manufactured DOEs recorded by a CCD-line array (pixel size is 14 μm). Figures 5 a) and 5 b) display the experimental rings intensity profile for two DOEs with a ring spacing of 1 mm and 0.5 mm, respectively. The intensity distributions for adjusting rings from one of the DOEs are presented in Fig.5c).

a)

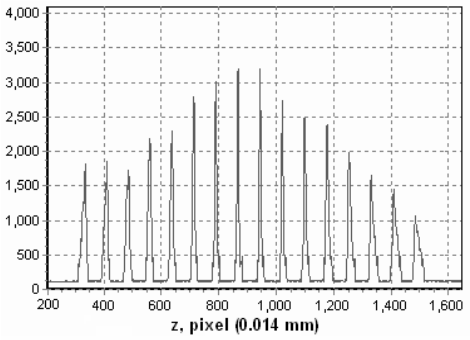

b)

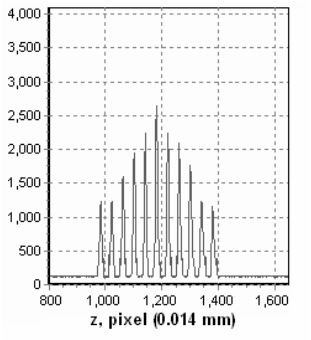

c)

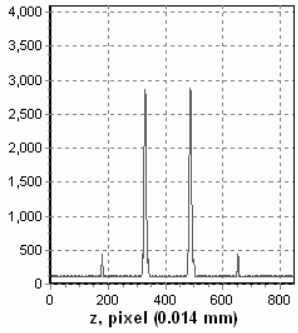

Fig.5 Experimental rings intensity for synthesized DOEs with ring spacings 1 mm (a) and 0.5 mm (b), adjusting rings (c)

It is sufficient to use four such diffractive elements with different diameters and spacing of light rings to inspect the entire range of grid spacers. The system adjustment for the inspection of various grid spacer types is performed by replacing the DOEs.

4. IMAGE-FORMING OBJECTIVE CALCULATION

The objective must project the illuminated inner surface of the cell to the camera matrix, and the light rings along the entire length of the cell must have good resolution. To perform this task, the field curvature and distortion of the objective must be specially increased.

A three-element projection objective was calculated with the use of special software for the calculation of optical systems Zemax-EE. The images of some grid spacer elements that must be inspected were simulated. Figures 6a) – c) demonstrate the special design objective performances, including the calculated spot diagram (a) and the fringes images for different grid spacer elements calculated by a ray tracing method for the following cases: protrusion fringe image for 2 mm radius protrusion (b), cylinder fringe image for 9 mm cylinder diameter (c). Figure 6 d) shows a real grid spacer cell inner surface image (grey zone) formed in white light by the abovementioned manufactured objective (black spot in the middle is a filter built-in the objective to cut off the of DOE zero order diffraction).

A deliberate increase of the objective field curvature is achieved by introducing astigmatism. Figure 6 a) presents the geometrical spot diagram (impulse response) in the centre of the inspected cell (for the middle light ring). Due to line form of scattered spot, the structured light fringes are merging on the edges of protrusions (see Fig.6b). It does not

occur under the registration of fringes images because for all ring points the surface normal is perpendicular to the scattering spot. The resolution of structural illumination fringes (in the protrusion centre) with a spacing of 0.5 mm is practically a limiting value for this objective. In this case, the spatial resolution along CCD in the tangential direction equals 20–25 cycles mm^{-1}, in the sagittal one it is 2–8 cycles mm^{-1}.

a)

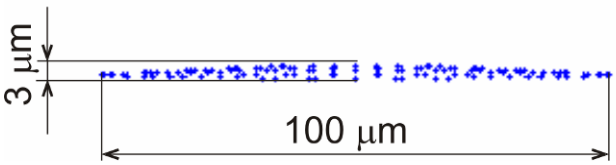

b)

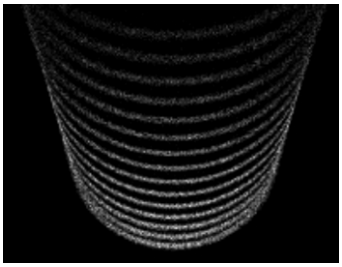

c)

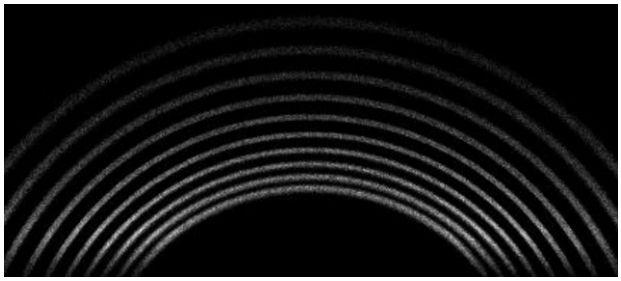

d)

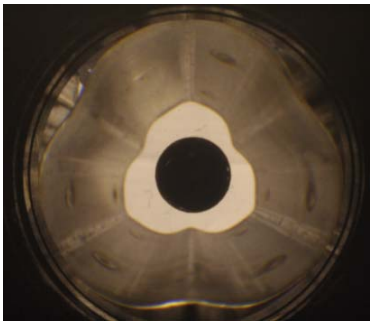

Fig.6 Illustrations of special design objective performances: the calculated spot diagram (a); the calculated fringe images under multiple-ring illumination for different grid spacer elements: the cell protrusion with 2 mm radius (b), the cylinder with 9 mm diameter (c); the real cell inner surface image (grey zone) formed by the designed objective (d)

5. IMAGE DIGITAL PROCESSING ALGORITHM

An algorithm for the calculation of the fringes location based on radial scanning of the output image from the optical axis was developed. Its essence is the following. First of all, the processed image is segmented in several sub-images with visible fringe patterns (corresponding to protrusion areas). Then the image is processed in polar coordinates with a centre at point x_0, y_0. The radial distribution of intensity $I(R)$ containing N peaks at the scanning direction is analyzed. The main task is to identify the peaks correctly and to find their coordinates. Figure 7 shows typical images of rings on different surfaces. Images were received using a CMOS sensor with 3456 × 2304 pixels (pixel size is 6.4 μm) and a semiconductor laser with an output power of 40 mW.

a)

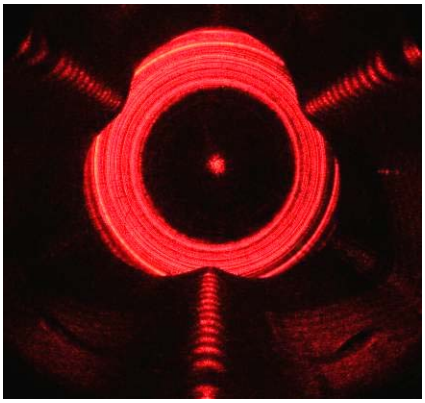

b)

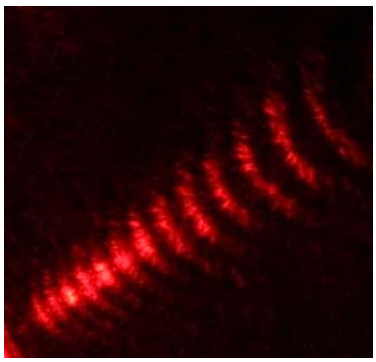

c)

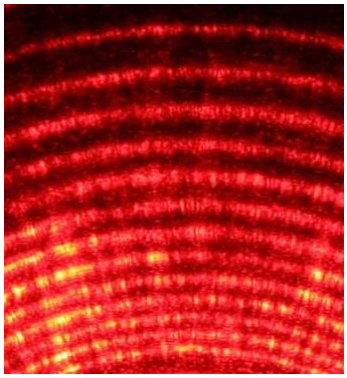

Fig.7 The experimental results: fringe images under multiple-ring illumination for a complete cell (a), a cell protrusion (b), a cylindrical hole with a diameter of 8.9 mm (c)

One can see from the photos (Figures 7a – 7c) that the ring images have some peculiarities that complicate the radial intensity distribution *I (R)* processing. The distance between the fringes is increased under the radius growth. The fringes intensity difference at the edge and the centre is considerable. Therefore the following methods are used to process the intensity distribution *I (R)* (see Fig.8). The averaged intensity distribution *I*ave*(R)* (background component) is calculated by means of the moving average method along *I (R)*, with a mask width larger than the fringe width. Then the background component is subtracted from the distribution *(I (R) − I*ave*(R))*. The distribution obtained is scaled with respect to *R*, so that the distances between the fringes are about the same, and approximated by a Fourier series. The number of harmonics of the series is chosen depending on the number ***N*** of fringes. The approximating curve *I*app*(R*m*)* has *N* peaks, which are used later to calculate the exact location of fringes using the mass centre method.

After the radial scanning is completed, the fringe numbers are checked. If fringes at some directions of scanning are determined incorrectly (not all fringes are determined, some fringes are omitted etc.), the fringe numbers are changed. If this is impossible, the points are removed and not considered later.

Before this procedure, the experimental system is calibrated. Using the workpieces, the distance *r* (from optical axis to inspected surface) dependence on image fringe radius *R* is determined. In other words, the calibration curve *rn(R)*, where *n* is the fringe number, for every ring is calculated.

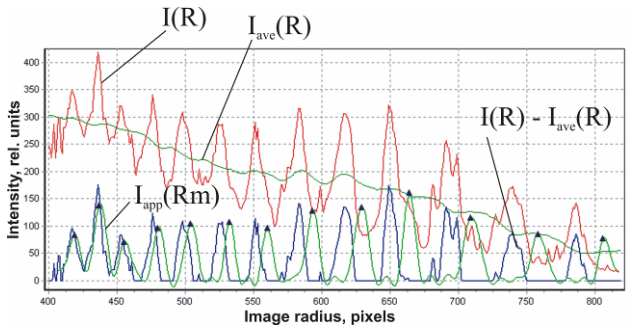

Fig.8 Processing of radial intensity distribution from protrusion

Let us consider an example of cell protrusion image processing. Under the inspection of grid spacer cells, three zones located at 120º (for hexagonal grid spacers) or four angular zones located at 90º (for square grid spacers) are radially scanned. The scanning zone size for one protrusion is 20º–30º. The scanning angle φ = 0.1º –0.125º. Each fringe on a protrusion is approximated by a third-order polynomial used to determine the fringe top. The top corresponds to the protrusion surface point that is the nearest to the axis. Figure 9(*a*) presents an example of image processing. One of the cell protrusions is shown. The fringes on the protrusion are denoted by a set of points through which approximating polynomials are drawn.

Figure 9b) shows the function *Ri(*φ*i)* for fringes on this protrusion with approximating polynomials. In the experiments, the angular size of fringes on protrusions was 4º – 8º and, hence, about 30–80 points were given to one protrusion. The images of the other grid spacer elements are processed similarly, with slight differences.

a)

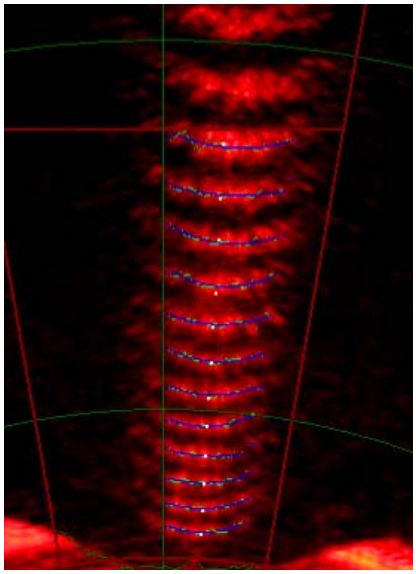

b)

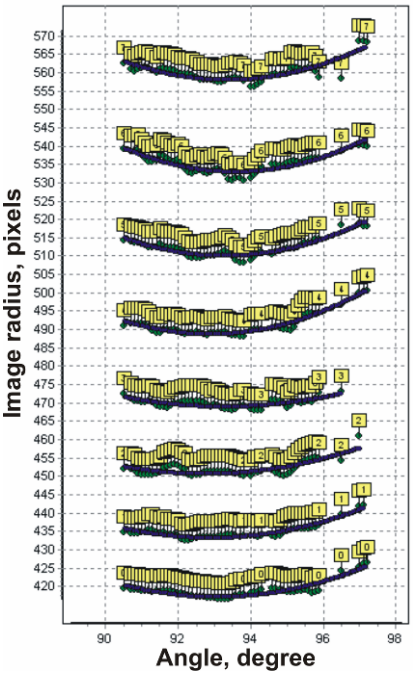

Fig.9 Cell images processing: processed protrusion image a), function $\mathbf{R_i(\varphi_i)}$ for protrusion fringes (b)

6. METHOD REALIZATION

A universal system for grid spacer geometrical parameters inspection was produced on the basis of the considered method. The general view of the system's opto-

mechanical unit is shown in Fig.10. It consists of a massive base with a two-coordinate table and an arch support. The illumination unit and capstan mechanism with DOE set are mounted on the arch. The inspected grid spacer is rigidly fixed in special mounting. The photoreceiver part with projection objective is placed inside the base. Two displacement sensors (on X, Y coordinates) are provided for precision determination of table displacement. The control of the system using the controller as well as data processing are performed by computer, placed on the working table of the operator.

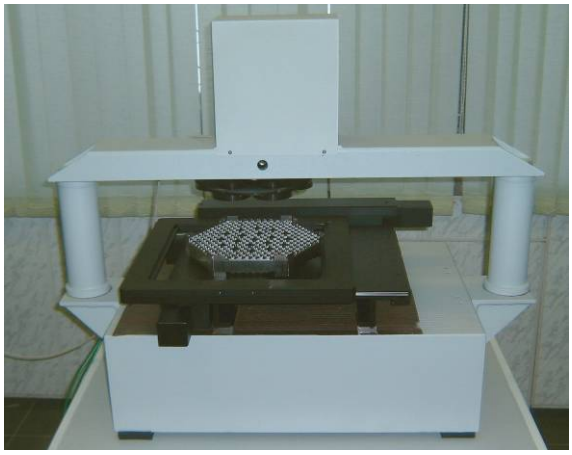

Fig.10 Opto-mechanical unit of measurement system

The developed software can be divided into three module types:

- control of system's hardware component;
- imaging the measurement results;
- image data processing, calculation of inspected objects parameters.

The software of the system's hardware component ensures the interaction with linear displacement sensors, a laser control unit, a CCD camera and a two-coordinate table controller. The database for measurement information storage and graphic interface for measurement results imaging was designed within the framework of software for displaying the spacer grid inspection results.

7. EXPERIMENTAL RESULTS

The experimental investigations were carried out on the measuring system for its metrological characteristics testing, using the special grid spacer prototypes. Only some prototypes selected from the serial products were used. In this case each prototype ensured the testing of the system's metrological characteristics within the defined range of parameters inspection for the determined types of grid spacers. The prototypes were measured provisionally with high accuracy (with error no more than 2 μm) on the coordinate-measuring machine (CMM). The grid spacer measurement results are shown in the Table 1. The obtained experimental results are in good agreement with the requirements imposed to the grid spacer measurement accuracy.

8. CONCLUSION

A universal method for grid spacers inspection based on using the diffractive optical elements for forming the structured illumination of grid surfaces was developed. This method allows us to perform reliable 3D-inspection of major grid spacer elements such as cells, channel holes, and rim. The system retuning for various types of cells is minimal and is reduces to replacement of diffractive elements.

Based on the developed method, the experimental prototype of a universal system for grid spacers' inspection was created. A software for the inspection system control, adjustment and calibration of the system optical part, as well as the algorithms for the image processing and calculation of the geometrical parameters grid spacer elements were developed. Experimental testing of the system showed the high metrological capabilities of the considered inspection method. The measurement error of inscribed cell circles diameters for hexagonal grid spacer with long protrusion and short protrusion was 3–4 μm. The measurement error of cell position shift for hexagonal grid spacer with long protrusion and short protrusion was 5–12 μm. As for the square grid spacer measurement, the distance error between opposite cell protrusions was 10 μm.

Table 1

Type of grid spacer	Inspected parameters	Measurement error, μm
Hexagonal grid spacer with long protrusion (15 mm)	Measurement error of inscribed cell circles diameters, **ΔDc**	± 3
	Measurement error of diameters of inscribed circles in channel holes, **ΔDch**	± 19
	Measurement error of cell position shift, **ΔL**	± 12
Hexagonal grid spacer with short protrusion (5 mm)	Measurement error of inscribed cell circles diameters, **ΔDc**	± 4
	Measurement error of diameters of inscribed circles in channel holes, **ΔDch**	± 8
	Measurement error of cell position shift, **ΔL**	± 5
Square grid spacer	Measurement distance error between opposite cell protrusions, **ΔDc**	± 10

REFERENCES

[1] Reshetnikov, F.G., Bibilashvili, Yu.K., Golovin, I.S. (1995). *Development, Production and Operation of TVEL Power Reactors*. Moskva: Energoatomizdat. (In Russian)

[2] Franke, E.A., Magee, M.J, Mitchell, J.N., Rigney, M.P. (2004). Three-dimensional precision surface measurement by dynamic structured light. In International Society for Optical Engineering, Vol. 5265, 2-6 August 2004 (pp. 24). Denver: SPIE.

[3] Bityutsky, O.I., Chugui, Yu.V., Gushchina, A.A., Kuchinsky, K.I., Ladygin, V.I., Plotnikov, S.V., Vertoprakhov, V.V., Yunoshev, V.P., Chapaev, I.G., Karlov, Yu.K., Rozhkov, V.V., Zarubin, M.G., Pimenov, Yu.V., Chernyshov, V.M. (2002). Laser measuring machine for 3D noncontact inspection of geometric parameters of grid spacers for nuclear reactors VVER-1000. In Proceedings of SPIE, Vol. 4900 (pp. 202-212). Bellingham: SPIE.

[4] Soifer, V.A. (ed.) (2000). *Metodi kompyuternoi optiki.* Moskva: Fizmatlit (In Russian)

[5] Kiryanov, V.P. (1997). Laser setup for flat optical components fabrication with submicron resolution. In Proceedings of SPIE, Vol. 3091 (pp. 66-70). Bellingham: SPIE.